Quantum Information Processing (2020) 19:118
https://doi.org/10.1007/s11128-020-2614-x

Topological quantum walks in cavity-based quantum networks

Ya Meng[1,2] · Feng Mei[1,2] · Gang Chen[1,2,3] · Suo-Tang Jia[1,2]

Received: 1 March 2019 / Accepted: 18 January 2020

Abstract

We present a protocol to implement discrete-time quantum walks and simulate topological insulator phases in cavity-based quantum networks, where a single photon is the quantum walker and multiple cavity input–output processes are employed to realize a polarization-dependent translation operation. Different topological phases can be simulated through tuning the single-photon polarization rotation angles. We show that both the topological boundary states and topological phase transitions can be directly observed via measuring the final photonic density distribution. Moreover, we also demonstrate that these topological signatures are quite robust to practical imperfections. Our work opens a new prospect using cavity-based quantum networks as quantum simulators to study discrete-time quantum walks and mimic condensed matter physics.

Keywords Topological quantum walk · Cavity input–output process · Topological boundary states · Topological phase transition

✉ Feng Mei
meifeng@sxu.edu.cn

✉ Gang Chen
chengang971@163.com

Ya Meng
mengya418@163.com

1 State Key Laboratory of Quantum Optics and Quantum Optics Devices, Institute of Laser Spectroscopy, Shanxi University, Taiyuan 030006, Shanxi, China

2 Collaborative Innovation Center of Extreme Optics, Shanxi University, Taiyuan 030006, Shanxi, China

3 Collaborative Innovation Center of Light Manipulations and Applications, Shandong Normal University, Jinan 250358, China

Published online: 18 February 2020

1 Introduction

Cavity input–output process is one of the basic building blocks in cavity quantum electrodynamics (QED) [1,2]. It has been widely used in studying quantum optics and cavity-based quantum information processing [3–16]. One of seminal protocols in this regard is the Duan–Kimble model [7], which has been extensively studied in the past years. In this model, a flying single photon has been input into an optical cavity with a single atom trapped inside. When the coupling between the single atom and photon is in the strong coupling regime, this cavity input–output process can function as a atom-photon-controlled phase flip gate. Recent experiments have successfully demonstrated the Duan–Kimble model and also the controlled phase flip gates [17,18]. The setup in this model can also be used for single-photon transistor [19] and naturally scaled up to a cavity-based quantum network [3], where different cavity-based quantum nodes are connected by the flying photons. These progresses greatly promote the development of cavity-based quantum networks for scalable quantum computation [17,18,20–22].

On the other hand, investigating the discrete-time quantum walk (DTQW) in various quantum systems has recently attracted a lot of research attentions, including in photons [23–30], cold atoms [31–34], trapped ions systems [35,36], and superconducting circuits systems [37,38]. Quantum walk is a quantum analog of the classical random walk [39]. Because of the coherence of the quantum states, the information propagates at a ballistic rate rather than a diffusive one in the classical random walks [40]. The DTQW also can provide a powerful tool to realize quantum computation [41] and quantum state transfer [42]. In addition to quantum information science, the DTQW also can function as a versatile quantum simulator for studying quantum diffusion, Anderson localization and topological phases [43–50]. For the quantum simulation of topological phases, many recent research attentions have been paid to investigate the topological boundary states and the topological phase transition via DTQWs in linear optics and optical lattice systems [51–63]. However, such topological features have not been explored in a cavity-based quantum network, which we will argue has several important benefits.

In this paper, motivated by the recent experiments on cavity input–output process, we propose a protocol using a cavity-based quantum network as a quantum simulator to realize a single-photon DTQW. In this protocol, the polarization-dependent translation operation which is the basic ingredient for implementing DTQWs can be achieved by multiple cavity input–output processes. Based on this DTQW, we further show that a one-dimensional topological phase characterized by a pair of topological winding numbers can be simulated via many steps of this DTQW in a cavity-based quantum network. The topological phase diagram versus the rotation angles is also given. We further study the topological features of this DTQW, including the topological boundary states and the topological phase transitions. In particular, we illustrate how to design a cavity-based quantum network with two different topological phases and observe the emerged topological boundary states. All the topological phase transition points between different topological phases can be unambiguously measured from the final output photonic density distribution. Our results are also robust to the imperfections in each step of cavity-assisted quantum walks.

This paper is structured as follows. In Sect. 2, we show how to realize DTQW using multiple cavity input–output processes in a cavity-based quantum network. In Sect. 3, we analyze the topological structure of our DTQW. In Sect. 4, we illustrate how to create and observe the topological boundary states in such network. In Sect. 5, we demonstrate the topological phase transition can also be directly observed in this quantum simulator. In Sect. 6, we give a conclusion to summarize our work.

2 DTQWs via multiple cavity input–output processes

We consider a single-photon DTQW, which is governed by an one-step unitary operator

$$\hat{U}(\theta_1, \theta_2) = \hat{R}_y\left(\frac{\theta_1}{2}\right)\hat{T}\,\hat{R}_y(\theta_2)\hat{T}\,\hat{R}_y\left(\frac{\theta_1}{2}\right), \tag{1}$$

where $\hat{R}_y(\theta_i) = \mathrm{e}^{-i\hat{\sigma}_y\cdot\frac{\theta_i}{2}}$ $(i = 1, 2)$ are the single-photon polarization rotation operations. $\hat{T}$ is a polarization-dependent translation operation

$$\hat{T} = \sum_x |x+1\rangle\langle x| \otimes |R\rangle\langle R| - |x-1\rangle\langle x| \otimes |L\rangle\langle L|, \tag{2}$$

where $|R\rangle(|L\rangle)$ is the right-circular (left-circular) polarization of a single photon, and $|x\rangle$ denotes the discrete position in one dimension. This translation operator is unique from that usually found in the literature [43,44]: a minus sign on the second term due to the phase shift. As illustrated in Fig. 1a, such a single-photon DTQW can be implemented in a cavity-based quantum network.

The basic building block in our protocol is the input–output process of one single cavity, which consists of a two-level atom trapped in a two-side optical cavity, see Fig. 1b–c. The cavity has two resonant modes a_R and a_L, with right-circular (R) and left-circular (L) polarizations, respectively. The input single-photon pulse contains two polarization components $|R\rangle$ and $|L\rangle$. The atomic transition $|g\rangle \leftrightarrow |e\rangle$ is resonantly coupled to the cavity mode a_R and is resonantly driven by the R polarization component of the input single-photon pulse. The L polarization component of the input pulse will see an empty cavity as the atom is decoupled to the cavity mode a_L. When the atom is prepared in the state $|g\rangle$, as we will demonstrate below, the L component of the input single-photon pulse is resonant with the bare cavity mode a_L and thus will go through the cavity with a phase of $\mathrm{e}^{i\pi}$. However, for the R component of the input single-photon pulse, with the strong atom-cavity coupling, the frequency of the dressed cavity mode is notably detuned from the frequency of the input single-photon pulse; thus, the R component will be reflected when it enters the cavity without a phase change.

For a detailed theoretical derivation, we give the interaction Hamiltonian of the atom and the cavity mode

$$\hat{H} = g(|e\rangle\langle g|a_R + |g\rangle\langle e|a_R^\dagger), \tag{3}$$

where g is the atom-cavity coupling rate. The cavity modes $a_\eta(\eta = R, L)$ are driven by the corresponding input fields $a_{\eta,l}^{\mathrm{in}}$ from the left side of the cavity. The Heisenberg–

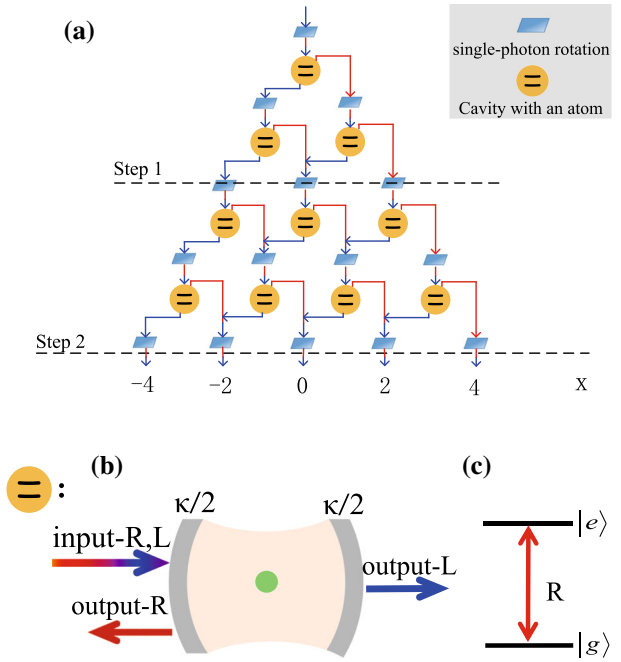

Fig. 1 **a** Schematic setup for the implementation of a single-photon DTQW in a cavity-based quantum network. The walker is a single photon with the red (blue) color denoting the right(left)-circular polarization $R(L)$ component of the single photon. The polarization-dependent translation $\hat{T}$ is implemented by multiple cavity input–output processes. The rotation operations $\hat{R}_y(\theta_i) = \mathrm{e}^{-i\hat{\sigma}_y\cdot\theta_i/2} (i = 1, 2)$ are implemented by the suitable wave plates, which could generate a superposition of left- and right-circularly polarized light. Since the rotation operation satisfy the relation $\hat{R}_y(\theta_1/2)\hat{R}_y(\theta_1/2) = \hat{R}_y(\theta_1)$, only one rotation operation is needed between adjacent steps during a multistep DTQW process. In order to spatially separate the reflected photon from the incident photon, a mirror, one side of which has high transmissivity and the other side has high reflectivity, is set in front of each atomic cavity. For simplicity, these mirrors are not shown here. **b** Schematic setup for a single cavity input–output process. A single two-level atom is trapped at the center of a two-side symmetric optical cavity, with decay rate $\kappa/2$ for each side, and thus, a total decay rate of κ. The L component of input photons can go through the cavity but the R component will be reflected when it enters the cavity. **c** Level structure of the two-level single atom and its coupling with the cavity mode a_R (Color figure online)

Langevin equations for the cavity modes a_η and the atomic operator have the form

$$\dot{a}_\eta = -i[a_\eta, \hat{H}] - \left(i\delta + \frac{\kappa}{2}\right) a_\eta - \sqrt{\frac{\kappa}{2}} a^{\mathrm{in}}_{\eta,l}, \tag{4}$$

where κ is the total decay rate of the cavity and δ denotes the detuning of the cavity field mode from the atomic transition. The cavity input–output relation connects the output fields $a^{\mathrm{out}}_{\eta,r}, a^{\mathrm{out}}_{\eta,l}$ with the input fields as

$$a^{\mathrm{out}}_{\eta,r} = \sqrt{\kappa/2} a_\eta, \tag{5}$$

$$a_{\eta,l}^{\text{out}} - a_{\eta,l}^{\text{in}} = \sqrt{\kappa/2}a_{\eta}. \tag{6}$$

We note that there is no input from right-side of the cavity.

For the L component of the input pulse, the Hamiltonian $\hat{H}$ in Eq. (4) does not work [7]. Suppose the input pulse shape changes slowly with time t compared with the cavity decay rate κ, that is $\dot{a}_{\eta} = 0$, from Eqs. (4)–(6), we can find

$$a_{L,r}^{\text{out}} = -\frac{\kappa/2}{i\delta + \kappa/2}a_{L,l}^{\text{in}}, \qquad a_{L,l}^{\text{out}} = \frac{i\delta}{i\delta + \kappa/2}a_{L,l}^{\text{in}}, \tag{7}$$

$$a_{R,l}^{\text{out}} = \frac{i\delta}{i\delta + \kappa/2}a_{R,l}^{\text{in}}, \qquad a_{R,r}^{\text{out}} = -\frac{\kappa/2}{i\delta + \kappa/2}a_{R,l}^{\text{in}}. \tag{8}$$

Therefore, for the resonant interaction $\delta = 0$, the transmission coefficient of the L component $T_L = a_{L,r}^{\text{out}}/a_{L,l}^{\text{in}} = |T_L|e^{\theta_T} = -1$ and the reflection coefficient $R_L = a_{L,l}^{\text{out}}/a_{L,l}^{\text{in}} = 0$, so the L component will go through the cavity and acquire a π phase shift. However, for the R component, the coupling (3) modifies the response function of the cavity. For the case of strong coupling, the two dressed cavity modes have frequencies that are effectively detuned from that of the input pulse by $\delta = \pm g$, respectively. When $g \gg \kappa$, we have the reflection coefficient of the R component $R_R = a_{R,l}^{\text{out}}/a_{R,l}^{\text{in}} = |R_R|e^{i\theta_R} = 1$, and the transmission coefficient $R_T = a_{R,r}^{\text{out}}/a_{R,l}^{\text{in}} = 0$, so the R component will be reflected without a phase change. By using multiple such cavity input–output processes, we can realize a polarization-dependent translation operation $\hat{T} = \sum_x R_R|x+1\rangle\langle x| \otimes |R\rangle\langle R| + T_L|x-1\rangle\langle x| \otimes |L\rangle\langle L|$, see Fig. 1a.

Very recently, such cavity input–output process has been experimentally demonstrated in a single-side cavity with a trapped single atom [17,18,20–22]. For the experimental implementation of our protocol, one could employ a single ^{87}Rb atom trapped in a three-dimensional optical lattice at the center of a two-sided optical high-finesse cavity. The relevant atomic transition could be chosen as $|g\rangle = |F = 2, m_F = 2\rangle \leftrightarrow |e\rangle = |F = 3, m_F = 3\rangle$, where F and m_F are the quantum numbers describing the total atomic angular momentum and its projection onto the quantization axis, respectively. The photons as well as the empty cavity are on resonance with the transition $|g\rangle \leftrightarrow |e\rangle$ at 780 nm. Based on such process, we can realize a polarization-dependent photonic translation.

Different from the DTQW using photons in linear optics [51–60], where the photonic state-dependent translation is generated by classical polarization-dependent optical elements, here the moving of photons is controlled by a quantum atom-photon coupling and its moving direction dependents on both the atomic and photonic internal states, which is important for studying and understanding the coherent features of quantum walks. Moreover, the atom-photon interaction can be flexibly tuned in current quantum optics laboratory, which offers more possibilities for designing and studying novel quantum walks. For example, our protocol can be directly generalized to realize a quantum walk with four internal quantum states in the coins by taking into account the two internal states in the atoms and photons. Specifically, we consider replacing the two-level single atoms with three-level single atoms, with two low-lying energy levels coupled with the upper excited state through left and right polarization cavity modes,

respectively. In this case, the two low-lying energy levels and the two photonic states form the four internal coin states. Combined with single photon rotation, it allows us to simulate complicated four-by-four spin-orbital couplings. Such spin-orbital couplings have not been realized in any artificial systems, which are important in realizing Z_2 topological insulator phases. Our study thus opens possibilities for realizing tunable complicated spin-orbital couplings and provides a promising platform for exploring Floquet Z_2 topological insulator phases. Furthermore, our setup can also be generalized to coherent state case, which can cause state-dependent moving and phase shifts on the coherent state, which allows us to explore novel topological quantum walks associated with atoms and coherent states. This can not be done for linear optics systems.

3 Topological features of the cavity-based quantum walks

In this section, we will analyze the topological features of our DTQW. As shown in Eq. (1), the unitary operator for the DTQW is equivalent to the evolution operator generated by a time-independent effective Hamiltonian $\hat{H}_{\text{eff}}$ over a step time δt [43,44], i.e., $\hat{U} = \mathrm{e}^{-i\hat{H}_{\text{eff}}\delta t}$. After N steps of DTQW, the evolution operator becomes $(\hat{U})^N = \mathrm{e}^{-i\hat{H}_{\text{eff}}N\delta t}$. In this case, the resulted DTQW simulates the evolution of an effective Hamiltonian $\hat{H}_{\text{eff}}$ at the discrete times $N\delta t$. In the following, we take the step time of DTQW as $\delta t = 1$. Using the Fourier transformation $|x\rangle = 1/\sqrt{2\pi}\sum_k \mathrm{e}^{ikx}|k\rangle$, the polarization-dependent translation operation can be written as $\hat{T}(k) = [\mathrm{e}^{ik}, 0; 0, -\mathrm{e}^{-ik}]$. Thus, the one-step DTQW operator in momentum space is $\hat{U} = \int_{-\pi}^{\pi} \mathrm{d}k \cdot \hat{U}(k) \otimes |k\rangle\langle k|$, where $\hat{U}(k) = \hat{R}_y(\theta_1/2)\hat{T}(k)\hat{R}_y(\theta_2)\hat{T}(k)\hat{R}_y(\theta_1/2)$. Furthermore, the effective Hamiltonian in momentum space has the form

$$\hat{H}_{\text{eff}} = \int_{-\pi}^{\pi} \mathrm{d}k[E(k)\mathbf{n}(k)\cdot\sigma] \otimes |k\rangle\langle k|, \tag{9}$$

where $\sigma = (\hat{\sigma}_x, \hat{\sigma}_y, \hat{\sigma}_z)$ are the Pauli matrices defined on the photonic polarization basis, $E(k)$ and $\mathbf{n}(k)$ are the quasienergies and the unit vector field, respectively. Through the relation $\hat{U}(k) = \mathrm{e}^{-iE(k)\mathbf{n}(k)\cdot\sigma}$, we can obtain the explicit forms of the eigenvalues and the spinor eigenstates

$$\begin{aligned} \cos E(k) &= \cos\frac{\theta_2}{2}\cos\frac{\theta_1}{2}\cos 2k + \sin\frac{\theta_2}{2}\sin\frac{\theta_1}{2}, \\ \mathbf{n}(k) &= \left(0, \frac{\cos\frac{\theta_2}{2}\sin\frac{\theta_1}{2}\cos 2k - \sin\frac{\theta_2}{2}\cos\frac{\theta_1}{2}}{\sin E}, -\frac{\cos\frac{\theta_2}{2}\sin 2k}{\sin E}\right). \end{aligned} \tag{10}$$

Note that the effective Hamiltonian possesses a chiral symmetry $\hat{\Gamma}^{-1}\hat{H}_{\text{eff}}\hat{\Gamma} = -\hat{H}_{\text{eff}}$, where the chiral operator $\hat{\Gamma} = \mathbf{A}\cdot\sigma$, the vector $\mathbf{A} = (1, 0, 0)$ is perpendicular to $\mathbf{n}(k)$ for the whole first Brillouin zone.

To characterize the topological features of this system, we firstly need to obtain the topological phase diagram governed by $\hat{U}$. For one-dimensional DTQWs with chiral symmetry, the complete topological phase diagram includes the gapped phases,

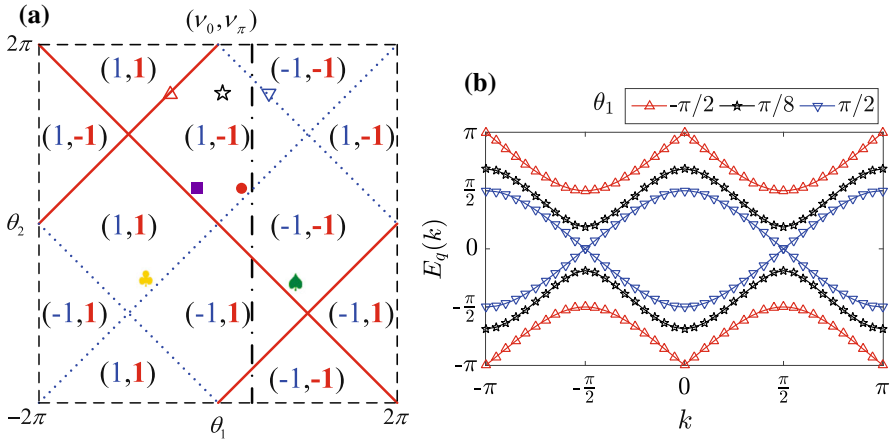

Fig. 2 **a** The topological phase diagram of the DTQW $\hat{U}(\theta_1, \theta_2)$. Different topological phases are characterized by (ν_0, ν_π). The phase boundaries correspond to points where the quasienergy gap closes at $E_q = 0$ (blue dotted lines) and $E_q = \pi$ (red solid lines). The dashed-dotted line indicates the rotation angles for observing the topological phase transition. The hollow-colored symbols indicate the rotation angles for plotting the quasienergy spectrum. The other colored symbols indicate the rotation angles for observing the topological boundary states. **b** The quasienergy spectrum of the cavity-based DTQW, where the rotation angles $\theta_{1,2}$ are chosen as the values in (**a**) (Color figure online)

characterized by a pair of topological winding numbers (ν_0, ν_π) [46,48], and the phase boundaries, which are determined by the quasienergies $E_q = \pm|E(k)|$.

For the phase boundaries, we know that the topological phase transition occurs at the gap closing point of the energy spectrum. Furthermore, the gap closes at quasienergies $E_q = 0$ as well as at $E_q = \pi$ due to the 2π periodicity in energy, which is unique to periodically driven systems. Through the explicit form of the quasienergies $E_q = \pm \arccos(\cos\frac{\theta_2}{2}\cos\frac{\theta_1}{2}\cos 2k + \sin\frac{\theta_2}{2}\sin\frac{\theta_1}{2})$, we can obtain the phase boundaries, see the blue dotted lines and the red solid lines in Fig. 2a. In Fig. 2b, we have plotted the quasienergies E_q as a function of quasimomenta k, where θ_2 is fixed at $3\pi/2$.

For the gapped phases, we need to consider another auxiliary one-step operator $\hat{U}'(\theta_1, \theta_2) = \hat{R}_y(\theta_2/2)\hat{T}\hat{R}_y(\theta_1)\hat{T}\hat{R}_y(\theta_2/2)$, and rewrite these one-step operators as

$$\hat{U}(\theta_1, \theta_2) = \mathrm{e}^{-i\pi}\hat{F}\cdot\hat{\Gamma}\hat{F}^\dagger\hat{\Gamma} = -\hat{U}_1, \tag{11}$$

$$\hat{U}'(\theta_1, \theta_2) = \mathrm{e}^{-i\pi}\hat{\Gamma}\hat{F}^\dagger\hat{\Gamma}\cdot\hat{F} = -\hat{U}_2, \tag{12}$$

where $\hat{F} = \hat{R}_y(\theta_1/2)\hat{T}\hat{R}_y(\theta_2/2)$, and $\hat{\Gamma} = \hat{\sigma}_x$. According to the method in [46,48], the pair of topological winding numbers (ν_0, ν_π) can be obtained through

$$(\nu_0, \nu_\pi) = (\tilde{\nu}_\pi, \tilde{\nu}_0) = \left(\frac{\nu_1 - \nu_2}{2}, \frac{\nu_1 + \nu_2}{2}\right), \tag{13}$$

where $(\tilde{\nu}_\pi, \tilde{\nu}_0)$ is a pair of topological winding numbers, which is used to characterize the topological gapped phases governed by the operators $\hat{U}_1$ and $\hat{U}_2$, and $\nu_1(\nu_2)$ is the winding number of the effective Hamiltonian governed by $\hat{U}_1(\hat{U}_2)$. Since the difference

between the operators $\hat{U}(\hat{U}')$ and $\hat{U}_1(\hat{U}_2)$ is just a minus sign, we can replace the winding numbers $\nu_1(\nu_2)$ with $\nu(\nu')$, which is the winding number of $\hat{U}(\hat{U}')$. For the operator $\hat{U}$, the winding number is defined as

$$\begin{aligned}\nu &= \frac{1}{2\pi}\int_{-\pi}^{\pi} \mathrm{d}k \left(\mathbf{n}\times\frac{\partial \mathbf{n}}{\partial_k}\right)\cdot\mathbf{A} \\ &= \frac{1}{2\pi}\int_{-\pi}^{\pi} \mathrm{d}k \left(n_y\frac{\partial n_z}{\partial_k} - n_z\frac{\partial n_y}{\partial_k}\right).\end{aligned} \tag{14}$$

Through numerical calculations, we can obtain the winding number ν as a function of the rotation angles θ_1 and θ_2. Similarly, we can calculate the winding number ν' for the operator $\hat{U}'$.

We have numerically calculated the topological phase diagram in Fig. 2a. One can find that various topological phases can be prepared via tuning the rotation angles θ_1 and θ_2. The topological phase transition occurs at the gap closing points at $E_q = 0$ as well as $E_q = \pi$. The number of boundary states at $E_q = 0(\pi)$ are equal to the difference of the winding numbers $\nu_0(\nu_\pi)$ in the two sides of the phase transition points, which yields the bulk-edge correspondence for topological quantum walks.

4 Observation of topological boundary states

According to the bulk-edge correspondence, boundary states will emerge at the boundaries between different topological phases [64,65]. Topological boundary states are one of basic signals showing the existence of topological phase. In this section, we will study three cases and show how to observe the topological boundary states generated at the boundaries. The boundary can be created by making the rotation angles θ_1, θ_2 spatially inhomogeneous in the cavity-based DTQW, such as (θ_1^l, θ_2^l) in the left region $x < 0$ and (θ_1^r, θ_2^r) in the right region $x \geq 0$.

In the first case, we consider two DTQW spatial regions with different rotation angles θ_1, θ_2, i.e., $(\theta_1^l, \theta_2^l) = (-\pi/4, 3\pi/8)$ and $(\theta_1^r, \theta_2^r) = (3\pi/4, -5\pi/8)$. As demonstrated in the last section, the topological invariants of the two regions are $(\nu_0, \nu_\pi) = (1, -1)$ and $(\nu_0, \nu_\pi) = (-1, -1)$, respectively. As the topological invariant ν_0 for the two regions are different, we expect to observe the topological boundary states with quasienergy $E_q = 0$ near the boundary $x = 0$. To experimentally observing such topological boundary states, a single photon pulse with polarization $1/\sqrt{2}(|R\rangle + |L\rangle)$ has been input into the cavity with position $x = 0$. Suppose this initial state is denoted as $|\psi(0)\rangle$. After that, as shown in Fig. 1a, we implement 15 steps of cavity-based DTQW governed by $\hat{U}$ and measure the final photon density distribution in the cavity outputs. In Fig. 3a, we have numerically calculated the final photon density distribution $P(x, N)$

$$P(x, N) = |\langle x, R|\psi(N)\rangle|^2 + |\langle x, L|\psi(N)\rangle|^2, \tag{15}$$

where the final state $|\psi(N)\rangle = \hat{U}^N|\psi(0)\rangle$. If there exists a topological boundary mode around the boundary $x = 0$, the input photon at $x = 0$ will resonate with this

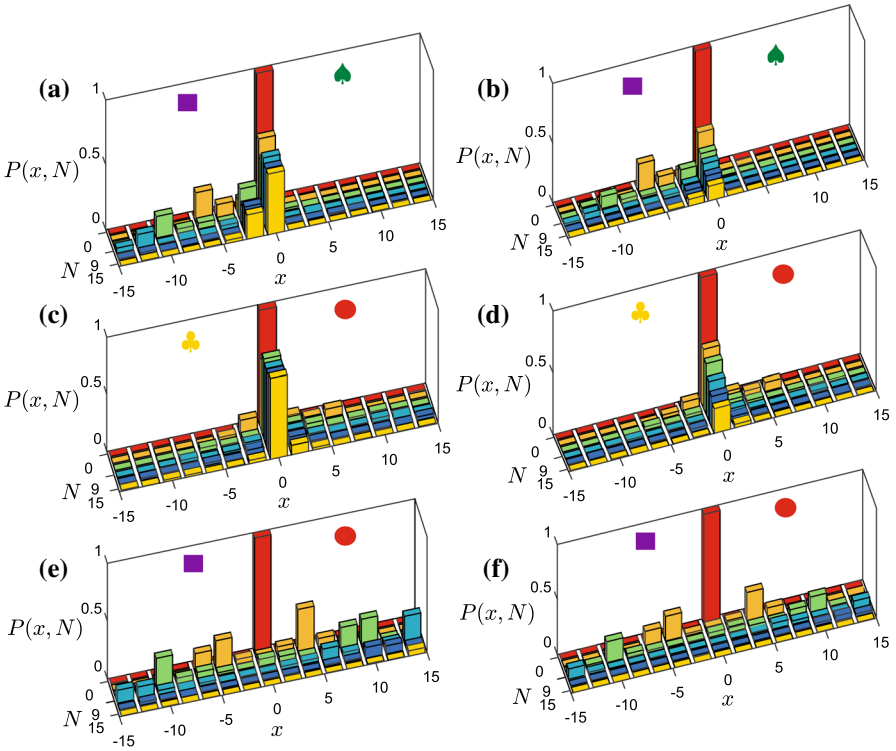

Fig. 3 The photon density distribution $P(x, N)$ of the inhomogeneous DTQW governed by $\hat{U}$ in the ideal **a**, **c**, **e** and realistic **b**, **d**, **f** cases when the number of steps is $N = 0, 3, 6, 9, 12, 15$. The colored symbols are consistent with those in Fig. 2a. Suppose the single-photon walker initially begins at the position $x = 0$. The polarization angles are **a**–**b** $(\theta_1^l, \theta_2^l) = (-\pi/4, 3\pi/8)$ and $(\theta_1^r, \theta_2^r) = (3\pi/4, -5\pi/8)$, **c**–**d** $(\theta_1^l, \theta_2^l) = (-3\pi/4, -5\pi/8)$ and $(\theta_1^r, \theta_2^r) = (\pi/4, 3\pi/8)$, **e**–**f** $(\theta_1^l, \theta_2^l) = (-\pi/4, 3\pi/8)$ and $(\theta_1^r, \theta_2^r) = (\pi/4, 3\pi/8)$. In the realistic case, the practical parameters in the state-dependent translation operation $\hat{T}$ are chosen as $R_R = 0.98 \cdot e^{i \cdot 0.05\pi}$ and $T_L = 0.98 \cdot e^{i \cdot 0.95\pi}$, and all the rotation angles have been introduced into a fluctuation $\Delta \in (-\pi/20, \pi/20)$ (Color figure online)

boundary mode and the final photon density will have a peak at $x = 0$. Our numerical result in Fig. 3a shows that the photon density distribution after 15 steps of DTQW is nonvanishing around the boundary $x = 0$, which indicates that the system has a topological boundary state at $x = 0$.

In the second case, we consider two DTQWs spatial regions $(\theta_1^l, \theta_2^l) = (-3\pi/4, -5\pi/8)$ and $(\theta_1^r, \theta_2^r) = (\pi/4, 3\pi/8)$. The topological invariants of the two regions are $(\nu_0, \nu_\pi) = (1, 1)$ and $(\nu_0, \nu_\pi) = (1, -1)$, respectively. As the topological invariant ν_π for the two regions are different, the topological boundary states with quasienergy $E_q = \pi$ are also expected in this case, which are confirmed by the numerical results shown in Fig. 3c.

In the third case, we consider creating a boundary between same topological phases, where the topological boundary state will not appear. For this purpose, the polarization angles θ_1, θ_2 in two DTQW spatial regions are tuned to $(\theta_1^l, \theta_2^l) = (-\pi/4, 3\pi/8)$ and

$(\theta_1^r, \theta_2^r) = (\pi/4, 3\pi/8)$. In this case, both the topological invariants in the two regions are $(\nu_0, \nu_\pi) = (1, -1)$, topological boundary states will not appear in the boundary $x = 0$. To demonstrate this point, we prepare the system into the same initial state $|\psi(0)\rangle$ as shown in the first two cases. In Fig 3e, the final photon density distribution after 15 steps of DTQW is numerically calculated. The distribution of the DTQW up to 15 steps shows ballistic behavior and no localization is observed around $x = 0$. It means that the system has no resonant topological boundary mode in the boundary $x = 0$.

Moreover, the novel topological features of a system are robust against small fluctuations. Thus, we also numerically calculate the influence of various imperfections in our protocol, which corresponds to the realistic case comparing with the ideal case (without imperfections). The imperfections mainly include the fluctuations of the parameters in $\hat{T}$ and $\hat{R}_y$ in each step of the cavity-assisted quantum walk [17,18,57,60]. For the translation operation $\hat{T}$, the experimental imperfections in the cavity input–output process will lead to the reduction of probability of the transmitted and reflected output pulse [17]. In addition, the fluctuations of the atomic, cavity and photon frequencies will lead to a variation of the phase of the transmitted and reflected output pulse [18]. For the rotation operation $\hat{R}_y$, the fluctuations on the rotation angles $\theta_{1,2}$ can be chosen randomly from the interval $[\bar{\theta}_{1,2} - \pi/20, \bar{\theta}_{1,2} + \pi/20]$ at every step of a DTQW, where $\bar{\theta}_{1,2}$ indicate the corresponding parameters without fluctuations [57,60]. The numerical results of the photon density distribution are shown in Fig. 3b, d, f. For the case supporting topological boundary states, the localization around the boundary of different topological phases decreases because of the loss of the cavity input–output process, but it remains maximal around the boundary. Then we still can unambiguously verify the existence of the topological boundary state even with various imperfections. For the case without topological boundary states, one still can find that there is no photons maximally localized around $x = 0$. So, due to the topological protection, the existence of the topological boundary states at the boundaries between different topological phases is robust against small perturbations.

5 Observation of topological phase transitions

In this section, we will further show that the topological phase transition between different topological phase can also be directly observed basing on second-order moment associated with final output photon density [58]. The rotation angles for observing topological phase transition are chosen as $\theta_1 = \pi/3$ and $\theta_2 \in [-2\pi, 2\pi]$. Similar to the last section, suppose the initial state of the system is prepared into $|\psi(0)\rangle$. To reveal the relationship between the topological phase transition and the final output photon density, the second-order moment is defined as [58]

$$M = \sum_x x^2 P(x, N)/N^2, \tag{16}$$

where $P(x, N)$ is the final output photon density distribution after N steps of DTQW. By transforming the above equation into momentum space, we further get

$$M = \int_{-\pi}^{\pi} \frac{\mathrm{d}k}{2\pi} \left\langle \psi(0)|(\hat{U}^{\dagger})^{N} \left(i\frac{\mathrm{d}}{\mathrm{d}k}\right)^{2} (\hat{U})^{N}|\psi(0)\right\rangle / N^{2}. \tag{17}$$

The N-step evolution operator can be expanded as $(\hat{U})^{N} = \mathrm{e}^{-i\hat{H}_{\mathrm{eff}}N} = \cos[N\cdot E] - i\sin[N\cdot E]\mathbf{n}\cdot\sigma$. Thus, we can obtain M in the following form

$$\begin{aligned} M = & \int_{-\pi}^{\pi} \frac{\mathrm{d}k}{2\pi} [\frac{\mathrm{d}E}{\mathrm{d}k}]^{2} \\ & + \frac{2i}{N} \int_{-\pi}^{\pi} \frac{\mathrm{d}k}{2\pi} \left\{ \frac{\mathrm{d}E}{\mathrm{d}k} \cos[N\cdot E] \left\langle \varphi_0|(\hat{U}^{\dagger})^{N} \frac{\mathrm{d}}{\mathrm{d}k}\mathbf{n}\cdot\sigma|\varphi_0\right\rangle \right\} \\ & + \frac{i}{N} \int_{-\pi}^{\pi} \frac{\mathrm{d}k}{2\pi} \left[\frac{\mathrm{d}^{2}E}{\mathrm{d}k^{2}} \langle\varphi_0|\mathbf{n}\cdot\sigma|\varphi_0\rangle \right] \\ & + \frac{i}{N^{2}} \int_{-\pi}^{\pi} \frac{\mathrm{d}k}{2\pi} \left\{ \sin[N\cdot E] \left\langle \varphi_0|(\hat{U}^{\dagger})^{N} \frac{\mathrm{d}^{2}}{\mathrm{d}k^{2}}\mathbf{n}\cdot\sigma|\varphi_0\right\rangle \right\}, \end{aligned} \tag{18}$$

where $|\varphi_0\rangle$ is the initial polarization state of the single photon.

Under the infinite-steps-limit, that is $N \to \infty$, we ignore these infinitesimal terms in Eq. (18). The form of M becomes particularly simple

$$M = \frac{1}{2\pi} \int_{-\pi}^{\pi} \left[\frac{\mathrm{d}E}{\mathrm{d}k}\right]^{2} \mathrm{d}k, \tag{19}$$

where the quasienergies $E = \arccos(\cos\frac{\theta_2}{2}\cos\frac{\theta_1}{2}\cos 2k + \sin\frac{\theta_2}{2}\sin\frac{\theta_1}{2})$. The above integral can be rewritten as $M = \oint f(z)\mathrm{d}z$ with the complex variable $z = \mathrm{e}^{i\cdot k}$, which can be analytically calculated using the residue theorem. After a long straightforward calculation, we obtain

$$M = \begin{cases} 2, & -2\pi < \theta_2 < -\frac{5\pi}{3}, \\ 4 + 4\sin\frac{\theta_2}{2}, & -\frac{5\pi}{3} < \theta_2 < -\frac{\pi}{3}, \\ 2, & -\frac{\pi}{3} < \theta_2 < \frac{\pi}{3}, \\ 4 - 4\sin\frac{\theta_2}{2}, & \frac{\pi}{3} < \theta_2 < \frac{5\pi}{3}, \\ 2, & \frac{5\pi}{3} < \theta_2 < 2\pi. \end{cases} \tag{20}$$

It turns out that the second-order moment has a plateau when the topological invariants $\nu_\pi = \nu_0$, in contrast to the sine oscillation when the topological invariants $\nu_\pi \neq \nu_0$. Such obvious difference allows us to observe a slope discontinuity at the topological phase transition points in the experiment.

In Fig. 4a–b, we have numerically calculated the second-order moment M as functions of the controllable polarization angle θ_2 for different steps of DTQW in the ideal case. It is found that M has a plateaus in the regions $\{-2\pi, -5\pi/3\}$, $\{-\pi/3, \pi/3\}$ and $\{5\pi/3, 2\pi\}$. According to the phase diagram, the topological invariants governed by cavity-based DTQW $(\hat{U})$ in these regions are $(\nu_0, \nu_\pi) = (-1, -1)$. In contrast, M has sine oscillations in the other regions where the topological invariants are

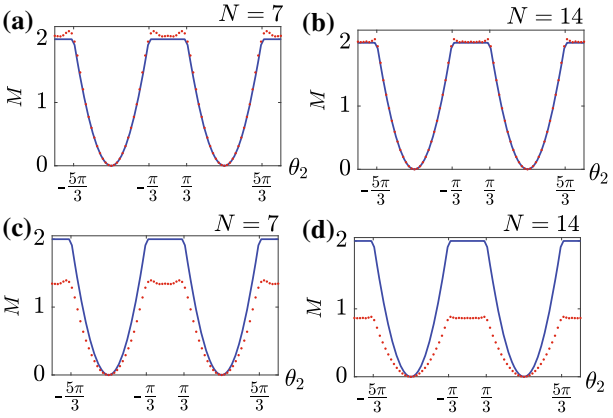

Fig. 4 The second-order moment varying with different polarization rotation angle θ_2 for the ideal **a**–**b** and realistic **c**–**d** cases. The parameters for the realistic case is chosen same as those in Fig. 3. The number of DTQW steps is (**a**, **c**) $N = 7$, (**b**, **d**) $N = 14$. The red dots (blue solid lines) denote the numerical (analytical) results (Color figure online)

$(\nu_0, \nu_\pi) = (-1, 1)$ or $(1, -1)$. Then the phase transition between different topological phases can be clearly observed from the slope discontinuity of M. We also show that M agrees very well with the theoretical predicated value in Eq. (20) when the number of quantum walk steps N become very large. We note that the behaviors of M in different topological regions ($\nu_\pi = \nu_0$ or $\nu_\pi \neq \nu_0$) depend on the parametric region chosen for observing topological phase transitions [60]. If the parametric region in our system are chosen as $\theta_2 = \pi/3$ and $\theta_1 \in [-2\pi, 2\pi]$, the corresponding M has a plateau when the topological invariants $\nu_\pi \neq \nu_0$ and has sine oscillations when the topological invariants $\nu_\pi = \nu_0$, which is consistent with the results in [58,60]. In Fig. 4c–d, we also calculate the influence of the cavity loss in each step of quantum walk on the above results. It turns out that, although the value of the plateaus changes, the plateaus remains in the presence of small imperfections. This feature has not been reported previously [58]. It shows that the second-order moment is quite robust against imperfections and also has a topological protection. Moreover, this method based on quantum dynamics of single particle state can be generalized to detect and explore various topological phases, including the non-equilibrium topological phases of matter.

6 Conclusion

In summary, we have proposed a protocol to implement single-photon DTQWs in cavity-based quantum networks. Multiple cavity input–output processes are employed to realize a polarization-dependent translation operation, which recently have been extensively studied in the quantum optics laboratory for implementing large-scale quantum network and scalable quantum computation [17,18,20–22]. We have shown how to employ cavity-based DTQWs as quantum simulators to mimic and explore the topological phases, including the topological boundary states and topological

phase transitions. Our work connects cavity-based quantum computation network with quantum simulation and can motivate more further studies on quantum simulation of condensed matter physics in this quantum platform.

Acknowledgements The work was supported by National Key R&D Program of China (2017YFA0304203); Natural National Science Foundation of China (11604392, 11674200, 11434007); Changjiang Scholars and Innovative Research Team in University of Ministry of Education of China (IRT_17R70); Fund for Shanxi "1331 Project" Key Subjects Construction; 111 Project (D18001).

References

1. Scully, M.O., Zubairy, M.S.: Quantum Optics. Cambridge University, Cambridge (1997)
2. Walls, D.F., Milburn, G.J.: Quantum Optics. Springer, Berlin (2010)
3. Reiserer, A., Rempe, G.: Cavity-based quantum networks with single atoms and optical photons. Rev. Mod. Phys. **87**, 1379 (2015)
4. You, J.-Q., Nori, F.: Atomic physics and quantum optics using superconducting circuits. Nature **474**, 589–597 (2011)
5. Xiang, Z.-L., Ashhab, S., You, J.-Q., Nori, F.: Hybrid quantum circuits: superconducting circuits interacting with other quantum systems. Rev. Mod. Phys. **85**, 623 (2013)
6. Gu, X., Kockum, A.F., Miranowicz, A., Liu, Y.-X., Nori, F.: Microwave photonics with superconducting quantum circuits. Phys. Rep. **718–719**, 1–102 (2017)
7. Duan, L.-M., Kimble, H.J.: Scalable photonic quantum computation through cavity-assisted interactions. Phys. Rev. Lett. **92**, 127902 (2004)
8. Duan, L.-M., Kuzmich, A., Kimble, H.J.: Cavity QED and quantum-information processing with "hot" trapped atoms. Phys. Rev. A **67**, 032305 (2003)
9. Wang, B., Duan, L.-M.: Implementation scheme of controlled SWAP gates for quantum fingerprinting and photonic quantum computation. Phys. Rev. A **75**, 050304 (2007)
10. Xue, P., Xiao, Y.-F.: Universal quantum computation in decoherence-free subspace with neutral atoms. Phys. Rev. Lett. **97**, 140501 (2006)
11. Xiao, Y.-F., Lin, X.-M., Gao, J., Yang, Y., Han, Z.-F., Guo, G.-C.: Realizing quantum controlled phase flip through cavity QED. Phys. Rev. A **70**, 042314 (2004)
12. Mei, F., Feng, M., Yu, Y.-F., Zhang, Z.-M.: Scalable quantum information processing with atomic ensembles and flying photons. Phys. Rev. A **80**, 042319 (2009)
13. Mei, F., Yu, Y.-F., Feng, X.-L., Zhang, Z.-M., Oh, C.H.: Quantum entanglement distribution with hybrid parity gate. Phys. Rev. A **82**, 052315 (2010)
14. Wang, H.-F., Zhu, A.-D., Zhang, S., Yeon, K.H.: Optically controlled phase gate and teleportation of a controlled-NOT gate for spin qubits in a quantum-dot-microcavity coupled system. Phys. Rev. A **87**, 062337 (2013)
15. Wang, H.-F., Zhu, A.-D., Zhang, S.: One-step implementation of a multiqubit phase gate with one control qubit and multiple target qubits in coupled cavities. Opt. Lett. **39**, 1489 (2014)
16. Li, G., Zhang, P.-F., Zhang, T.-C.: Entanglement of remote material qubits through nonexciting interaction with single photons. Phys. Rev. A **97**, 053808 (2018)
17. Reiserer, A., Kalb, N., Rempe, G., Ritter, S.: A quantum gate between a flying optical photon and a single trapped atom. Nature (London) **508**, 237–240 (2014)
18. Hacker, B., Welte, S., Rempe, G., Ritter, S.: A photon-photon quantum gate based on a single atom in an optical resonator. Nature (London) **536**, 193–196 (2016)
19. Chang, D.E., Sørensen, A.S., Demler, E.A., Lukin, M.D.: A single-photon transistor using nanoscale surface plasmons. Nat. Phys. **3**, 807–812 (2007)
20. Reiserer, A., Ritter, S., Rempe, G.: Nondestructive detection of an optical photon. Science **342**(6164), 1349–1351 (2013)
21. Welte, S., Hacker, B., Daiss, S., Ritter, S., Rempe, G.: Cavity carving of atomic Bell states. Phys. Rev. Lett. **118**, 210503 (2017)
22. Welte, S., Hacker, B., Daiss, S., Ritter, S., Rempe, G.: Photon-mediated quantum gate between two neutral atoms in an optical cavity. Phys. Rev. X **8**, 011018 (2018)

23. Peruzzo, A., Lobino, M., Matthews, J.C.F., Matsuda, N., Politi, A., Poulios, K., Zhou, X.-Q., Lahini, Y., Ismail, N., Worhoff, K., Bromberg, Y., Silberberg, Y., Thompson, M.G., OBrien, J.L.: Quantum walks of correlated photons. Science **329**(5998), 1500–1503 (2010)
24. Schreiber, A., Cassemiro, K.N., Potoček, V., Gábris, A., Mosley, P.J., Andersson, E., Jex, I., Silberhorn, C.: Photons walking the line: a quantum walk with adjustable coin operations. Phys. Rev. Lett. **104**, 050502 (2010)
25. Broome, M.A., Fedrizzi, A., Lanyon, B.P., Kassal, I., Aspuru-Guzik, A., White, A.G.: Discrete single-photon quantum walks with tunable decoherence. Phys. Rev. Lett. **104**, 153602 (2010)
26. Schreiber, A., Cassemiro, K.N., Potoček, V., Gábris, A., Jex, I., Silberhorn, C.: Decoherence and disorder in quantum walks: from ballistic spread to localization. Phys. Rev. Lett. **106**, 180403 (2011)
27. Schreiber, A., Gábris, A., Rohde, P.P., Laiho, K., Stefanak, M., Potoček, V., Hamilton, C., Jex, I., Silberhorn, C.: A 2D quantum walk simulation of two-particle dynamics. Science **336**(6077), 55–58 (2012)
28. Bian, Z.-H., Li, J., Qin, H., Zhan, X., Zhang, R., Sanders, B.C., Xue, P.: Realization of Single-qubit positive-operator-valued measurement via a one-dimensional photonic quantum walk. Phys. Rev. Lett. **114**, 203602 (2015)
29. Boutari, J., Feizpour, A., Barz, S., Di Franco, C., Kim, M.S., Kolthammer, W.S., Walmsley, I.A.: Large scale quantum walks by means of optical fiber cavities. J. Opt. **18**, 094007 (2016)
30. Su, Q.-P., Zhang, Y., Yu, L., Zhou, J.-Q., Jin, J.-S., Xu, X.-Q., Xiong, S.-J., Xu, Q.-J., Sun, Z., Chen, K.-F., Nori, F., Yang, C.-P.: Experimental demonstration of quantum walks with initial superposition states. npj Quantum Inf. **5**, 40 (2019)
31. Preiss, P.M., Ma, R., Tai, M.E., Lukin, A., Rispoli, M., Zupancic, P., Lahini, Y., Ialam, R., Greiner, M.: Strongly correlated quantum walks in optical lattices. Science **347**(6227), 1229–1233 (2015)
32. Karski, M., Förster, L., Choi, J.-M., Steffen, A., Alt, W., Meschede, D., Widera, A.: Quantum walk in position space with single optically trapped atoms. Science **325**(5937), 174–177 (2009)
33. Genske, M., Alt, W., Steffen, A., Werner, A.H., Werner, R.F., Meschede, D., Alberti, A.: Electric quantum walks with individual atoms. Phys. Rev. Lett. **110**, 190601 (2013)
34. Dadras, S., Gresch, A., Groiseau, C., Wimberger, S., Summy, G.S.: Quantum walk in momentum space with a Bose–Einstein condensate. Phys. Rev. Lett. **121**, 070402 (2018)
35. Schmitz, H., Matjeschk, R., Schneider, C., Glueckert, J., Enderlein, M., Huber, T., Schaetz, T.: Quantum walk of a trapped ion in phase space. Phys. Rev. Lett. **103**, 090504 (2009)
36. Zähringer, F., Kirchmair, G., Gerritsma, R., Solano, E., Blatt, R., Roos, C.F.: Realization of a quantum walk with one and two trapped ions. Phys. Rev. Lett. **104**, 100503 (2010)
37. Yan, Z.-G., Zhang, Y.-R., Gong, M., Yulin, W., Zheng, Y.-R., Li, S.-W., Wang, C., Liang, F.-T., Lin, J., Xu, Y., Guo, C., Sun, L.-H., Peng, C.-Z., Xia, K.-Y., Deng, H., Rong, H., You, J.-Q., Nori, F., Fan, H., Zhu, X.-B., Pan, J.-W.: Strongly correlated quantum walks with a 12-qubit superconducting processor. Science **364**(6442), 753–756 (2019)
38. Flurin, E., Ramasesh, V.V., Hacohen-Gourgy, S., Martin, L.S., Yao, N.Y., Siddiqi, I.: Observing topological invariants using quantum walks in superconducting circuits. Phys. Rev. X **7**, 031023 (2017)
39. Aharonov, Y., Davidovich, L., Zagury, N.: Quantum random walks. Phys. Rev. A **48**, 1687 (1993)
40. Venegas-Andraca, S.E.: Quantum walks: a comprehensive review. Quant. Inf. Proc. **11**(5), 1015–1106 (2012)
41. Lovett, N.B., Cooper, S., Everitt, M., Kendon, V.: Universal quantum computation using the discrete-time quantum walk. Phys. Rev. A **81**, 042330 (2010)
42. Kurzyński, P., Wòjcik, A.: Discrete-time quantum walk approach to state transfer. Phys. Rev. A **83**, 062315 (2011)
43. Kitagawa, T., Rudner, M.S., Berg, E., Demler, E.: Exploring topological phases with quantum walk. Phys. Rev. A **82**, 033429 (2010)
44. Kitagawa, T.: Topological phenomena in quantum walks: elementary introduction to the physics of topological phases. Quantum Inf. Proc. **11**(5), 1107–1148 (2012)
45. Asbóth, J.K.: Symmetries, topological phases, and bound states in the one-dimensional quantum walk. Phys. Rev. B **86**, 195414 (2012)
46. Asbóth, J.K., Obuse, H.: Bulk-boundary correspondence for chiral symmetric quantum walks. Phys. Rev. B **88**, 121406 (2013)
47. Tarasinski, B., Asbóth, J.K., Dahlhaus, J.P.: Scattering theory of topological phases in discrete-time quantum walks. Phys. Rev. A **89**, 042327 (2014)

48. Obuse, H., Asbóth, J.K., Nishimura, Y., Kawakami, N.: Unveiling hidden topological phases of a one-dimensional Hadamard quantum walk. Phys. Rev. B **92**, 045424 (2015)
49. Cedzich, C., Grünbaum, F.A., Stahl, C., Velázquez, L., Werner, A.H., Werner, R.F.: Bulk-edge correspondence of one-dimensional quantum walks. J. Phys. A **49**, 21LT01 (2016)
50. Ramasesh, V.V., Flurin, E., Rudner, M., Siddiqi, I., Yao, N.Y.: Direct probe of topological invariants using Bloch oscillating quantum walks. Phys. Rev. Lett. **118**, 130501 (2017)
51. Kitagawa, T., Broome, M.A., Fedrizzi, A., Rudner, M.S., Berg, E., Kassal, I., Aspuru-Guzik, A., Demler, E., White, A.G.: Observation of topologically protected bound states in photonic quantum walks. Nat. Commun. **3**, 882 (2012)
52. Xiao, L., Zhan, X., Bian, Z.-H., Wang, K.-K., Zhang, X., Wang, X.-P., Li, J., Mochizuki, K., Kim, D., Kawakami, N., Yi, W., Obuse, H., Sanders, B.C., Xue, P.: Observation of topological edge states in parity-time-symmetric quantum walks. Nat. Phys. **13**, 1117–1123 (2017)
53. Wang, B., Chen, T., Zhang, X.-D.: Experimental observation of topologically protected bound states with vanishing Chern numbers in a two-dimensional quantum walk. Phys. Rev. Lett. **121**, 100501 (2018)
54. Chen, C., Ding, X., Qin, J., He, Y., Luo, Y.-H., Chen, M.-C., Liu, C., Wang, X.-L., Zhang, W.-J., Li, H., You, L.-X., Wang, Z., Wang, D.-W., Sanders, B.C., Lu, C.-Y., Pan, J.-W.: Observation of topologically protected edge states in a photonic two-dimensional quantum walk. Phys. Rev. Lett. **121**, 100502 (2018)
55. Zhan, X., Xiao, L., Bian, Z.-H., Wang, K.-K., Qiu, X.-Z., Sanders, B.C., Yi, W., Xue, P.: Detecting topological invariants in nonunitary discrete-time quantum walks. Phys. Rev. Lett. **119**, 130501 (2017)
56. Xu, X.-Y., Wang, Q.-Q., Pan, W.-W., Sun, K., Xu, J.-S., Chen, G., Tang, J.-S., Gong, M., Han, Y.-J., Li, C.-F., Guo, G.-C.: Measuring the winding number in a large-scale chiral quantum walk. Phys. Rev. Lett. **120**, 260501 (2018)
57. Cardano, F., D'Errico, A., Dauphin, A., Maffei, M., Piccirillo, B., Lisio, C.D., Filippis, G.D., Cataudella, V., Santamato, E., Marrucci, L., Lewenstein, M., Massignan, P.: Detection of Zak phases and topological invariants in a chiral quantum walk of twisted photons. Nat. Commun. **8**, 15516 (2017)
58. Cardano, F., Maffei, M., Massa, F., Piccirillo, B., de Lisio, C., De Filippis, G., Cataudella, V., Santamato, E., Marrucci, L.: Statistical moments of quantum-walk dynamics reveal topological quantum transitions. Nat. Commun. **7**, 11439 (2016)
59. Barkhofen, S., Nitsche, T., Elster, F., Lorz, L., Gábris, A., Jex, I., Silberhorn, C.: Measuring topological invariants in disordered discrete-time quantum walks. Phys. Rev. A **96**, 033846 (2017)
60. Wang, X.-P., Xiao, L., Qiu, X.-Z., Wang, K.-K., Yi, W., Xue, P.: Detecting topological invariants and revealing topological transitions in discrete-time photonic quantum walks. Phys. Rev. A **98**, 013835 (2018)
61. Groh, T., Brakhane, S., Alt, W., Meschede, D., Asbóth, J.K., Alberti, A.: Robustness of topologically protected edge states in quantum walk experiments with neutral atoms. Phys. Rev. A **94**, 013620 (2016)
62. Mugrl, S., Celi, A., Massignan, P., Asbóth, J.K., Lewenstein, M., Lobo, C.: Topological bound states of a quantum walk with cold atoms. Phys. Rev. A **94**, 023631 (2016)
63. Sajid, M., Asbóth, J.K., Meschede, D., Werner, D., Alberti, A.: Creating anomalous Floquet Chern insulators with magnetic quantum walks. Phys. Rev. B **99**, 214303 (2019)
64. Hasan, M.Z., Kane, C.L.: Colloquium: topological insulators. Rev. Mod. Phys. **82**, 3045 (2010)
65. Qi, X.-L., Zhang, S.-C.: Topological insulators and superconductors. Rev. Mod. Phys. **83**, 1057 (2011)